HEAT AND MASS TRANSFER IN WOOD COMPOSITE PANELS DURING HOT PRESSING. PART II. MODELING VOID FORMATION AND MAT PERMEABILITY

Chunping Dai†
Senior Scientist and Group Leader

Changming Yu
Visiting Professor

and

Xiaoyan Zhou
Visiting Associate Professor
Wood Composites Group
Forintek Canada Corp.
2665 East Mall
Vancouver, B.C.
Canada V6T 1W5

(Received June 2004)

ABSTRACT

Theoretical models have been developed to predict the porosity and permeability of wood strand mats during consolidation. Based on the Poisson distribution of mat formation, the porosity model predicts the formation of both inside- and between-strand void volumes. It is proposed and predicted that the between-strand voids consist of voids between non-contact strand faces and voids around strand edges, with the former dominating in the early stage of consolidation and the latter dominating in the latter stage of consolidation. The permeability model is developed based on the Carman-Kozeny theory for porous materials. The model is compared and agrees with experimental results obtained from this study and from the literature. The results show mat permeability is mainly controlled by voids between strands instead of those inside strands. Mat density has a primary effect and strand size has a secondary but very important effect on mat porosity and permeability especially in the later stage of consolidation. Strand thickness has a stronger impact than strand width and length. Strand dimensions and mat permeability are shown to have significant effects on internal environmental conditions in wood composites during hot-pressing.

Keywords: Hot-pressing, wood composites, void volume, porosity, permeability, consolidation and modeling.

INTRODUCTION

In the preceding paper of this series (Dai and Yu 2004), a theoretical model was presented to predict mat environmental conditions based on the physics principles of mass and energy conservation, momentum of gas flow, thermodynamics, and resin curing kinetics. The mat conditions such as temperature, moisture content, and gas pressure were shown to be closely linked to basic mat properties including thermal conductivity and permeability. One of the knowledge gaps identified was the lack of fundamental understanding and experimental data of mat permeability. The permeability is crucial to hot pressing of wood composites because it controls the convective heat and mass transfer from surfaces to core, and the ease with which internal vapor evaporates from the mat center to its edges during pressing and from core to surfaces during press opening. Specifically, the former controls the rate of core temperature rise and therefore

† Member SWST.

resin curing rate, while the latter is a determining factor to minimize blows or blisters in finished boards and pressing time.

The importance of mat permeability has also been identified in other studies reported in a review by Bolton and Humphrey (1994). It was hypothesized that mat permeability was linked to the existence of voids between wood elements instead of those within them. Such a hypothesis was rationalized by the fact that the permeability of a mat is usually much higher than that of wood from which the mat is made. It was further speculated that both void volume and permeability should be governed by the shape of the wood elements and mat densification. Unfortunately, the void volume and its relationship to permeability were not subsequently investigated or published.

Hata et al (1993) and von Haas (1998) were among the very few researchers who investigated mat permeability using experimental approaches. Pre-pressed mats of resinated wood elements were regarded as a continuum and tested for their permeability. While certain empirical models between mat permeability, element geometry, and mat density were found based on the experimental data, the models' applications are limited by the condition under which the experiments were conducted. Particularly, the models cannot be generalized to predict the permeability of mats with different element geometry. This can become a major drawback for any heat and mass transfer model considering that wood composites can be made from a wide geometric mix of wood elements. A more generalized model of the permeability-void volume-mat density would therefore be highly desirable for analyzing the effects of wood element geometry on hot-pressing behavior and even product properties.

Indeed, the significance of understanding the voids inside composite mats and final products should go beyond mat permeability and heat and mass transfer. From a material standpoint, void volume is one of the three major components of wood composites, with the other two being wood elements and resin additives. Therefore voids ought to play a major role in defining both the processing and the performance of wood composites. While its importance has been widely acknowledged (e.g. Suchsland 1959; Humphrey and Bolton 1989; Zombori et al 2003; Carvalho et al. 2003; Wu and Lee 2002), void volume in wood composites is poorly defined probably due to the lack of experimental techniques and partially due to the complex nature of the mat structure.

The goal of this paper was to improve the fundamental understanding of wood composite processing. The specific objectives were:

- To develop a theoretical model to predict the changes of void volume inside the mat as a function of wood element size and mat densification;
- To present a generalized model to predict the mat permeability in terms of the void volume and wood element size;
- To validate the permeability model by comparing with experimental results; and
- To demonstrate the usefulness of the model for analyzing the effects of wood element size on hot-pressing process.

THEORETCAL MODELING

Wood composites may be structurally classified into two categories: veneer-based and strand-based. The former represents products such as plywood and laminated veneer lumber (LVL), which are made from layers of veneer. Because of the continuity of veneer layers, the structure and formation of voids in those products are relatively straightforward and hence not investigated in this study.

In contrast, strand-based composites, which broadly represent such products as oriented strandboard (OSB), parallel strand lumber (Parallam™), particleboard, and fiberboard, are made from discontinuous wood elements, i.e. strands, particles, and fibers. The element discontinuity and random forming process inevitably induce voids between the elements. In fact, voids are the dominant volumetric fraction of a mat during forming. The void fraction then experiences a drastic change during mat consolidation. While most voids are removed during the initial consolidation, a certain fraction of voids

always exists even after excessive densification. It is therefore conceivable that the formation and removal of voids are associated with strand discontinuity, mat formation, and densification. To model the void volume and further the permeability of mats, two general assumptions are made concerning the element geometry and the mat-forming process:

1) Original wood elements or strands in a mat are assumed to be rectangular in shape. Their dimensions are defined by length, width, and thickness.
2) Strands are formed following a random process in which their positions are randomly distributed over the mat area. Note that strand orientation can be either random or oriented/partially oriented.

Random mat structure

Despite their more or less uniform appearance, strand mats are random in structure. The random mat structure is attributed to the nature of mat-forming processes which may at best control the local distributions of strand mass but not the positions of individual strands. As a result, the number of strand overlaps varies from one location to another. To illustrate such structure variations, we developed a computer simulation model using basic geometric theories (Dai and Steiner 1994b; Dai et al. 1996). Figure 1 shows simulated distributions of strand overlaps in a randomly formed strand layer and in a multilayered strand mat. The local strand overlaps vary from 0 to 5 in the single layer (Fig. 1a), and from 1 to 16 around the average of 10 strand overlaps in the multi-layer mat (Fig. 1b). In theory, the relationship between the strand overlaps i and their average n is governed by a Poisson distribution (Dai and Steiner 1994b; Dai et al. 1996). The probability of any given point in the mat covered by i strands, $p(i)$, is:

$$p(i) = \frac{a_i}{A} = \frac{e^{-n} n^i}{i!} \tag{1}$$

where: a_i = sum of mat areas in which the strand overlaps equal i [m^2],
A = overall mat area [m^2], and
n = average number of strand overlaps.

Equation (1) establishes an important linkage between the random strand overlaps to their corresponding mat areas. It allows for derivation of such mat structural properties as strand bonded area (Dai and Steiner 1993), horizontal density distribution (Dai and Steiner 1997), and void volume, which is to be analyzed in this paper.

The average strand overlap n is further defined by:

$$n = \frac{\lambda \omega N_f}{A} \tag{2}$$

where: λ = strand length [m],
ω = strand width [m], and
N_f = total number of strands in a mat.

Since mat density ρ_m [kg/m^3] is defined by:

$$\rho_m = \frac{\lambda \omega \tau \rho_s N_f}{TA} \tag{3}$$

where: τ = strand thickness [m],
ρ_s = original wood density of strands [kg/m^3], and
T = mat thickness [m], the average strand overlaps n can be further calculated by combining Eqs. (2) and (3):

$$n = \frac{\rho_m T}{\rho_s \tau} \tag{4}$$

or simply:

$$n = C_r T_r \tag{5}$$

where: C_r = compaction ratio or ρ_m/ρ_s, indicating the degree of mat consolidation, and
T_r = thickness ratio or T/τ.

Equations (1) and (5) suggest that the distribution of strand overlaps in randomly formed mats can be fully described if the mat compaction ratio and the thickness ratio are known. The greater the compaction ratio and the thickness ratio, the more uniform the mat (Dai and Steiner 1997). The Poisson distribution is a mat structure property, which is in fact independent of strand length, width, and mat size.

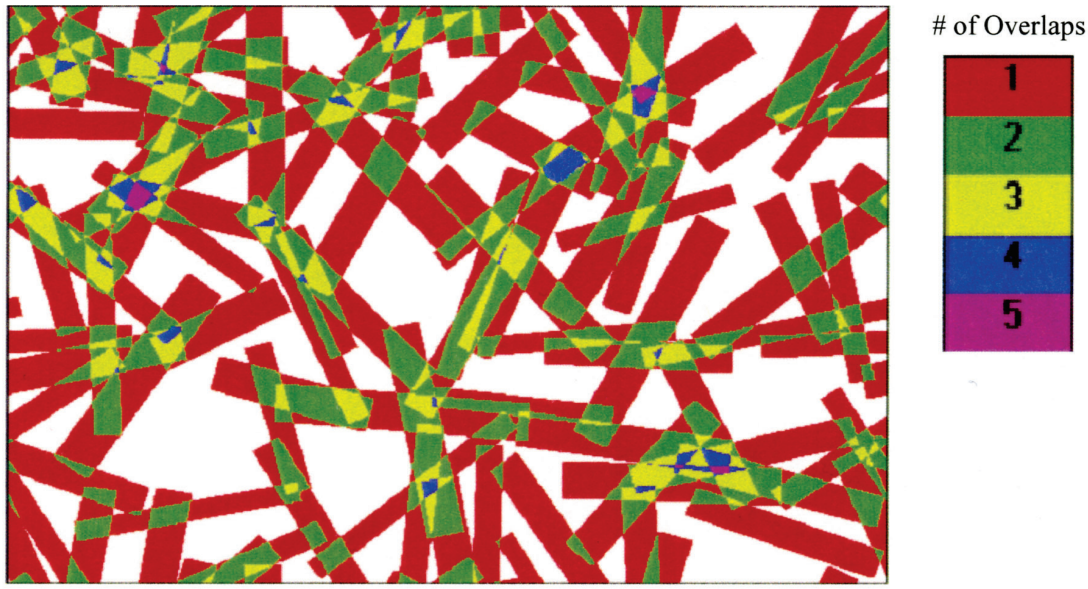

Fig. 1a

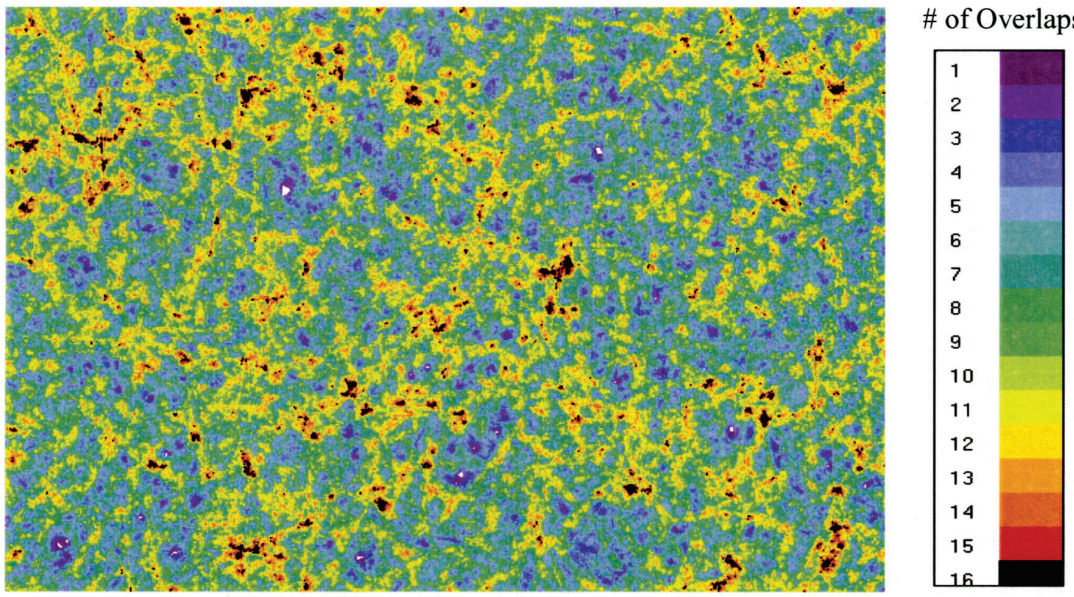

Fig. 1b

FIG. 1. Computer-simulated mat formation showing the variations of strand overlaps in: a). a single layer (average of one overlap), and b). a multi-layered mat (average of 10 strand overlaps).

Void formation

Since wood is a cellular material, voids in a strand mat can exist both between strands and inside strands. The *between-strand porosity,* ϕ_b, is defined as the ratio of void volume between strands over the total mat volume. The *inside-strand porosity,* ϕ_i, is defined as the ratio of void volume inside strands over the total mat volume. The total porosity in a mat, ϕ_t, is obviously equal to the sum of the two porosities, or:

$$\phi_t = \phi_b + \phi_i \tag{6}$$

Assume the cell-wall density, ρ_c, is known (usually around 1500 kg/m^3). The total mat porosity can be calculated by:

$$\phi_t = 1 - \frac{\rho_m}{\rho_c} \tag{7}$$

Equation (7) implies that ϕ_t can be calculated given that ρ_m is known (Eq.3). According to Eq. (6), ϕ_b or ϕ_i can be calculated if the other is known. The following analyses will only focus on the derivation of between-strand porosity ϕ_b.

Voids between strands are first induced during mat forming and can then be largely removed during mat consolidation. Due to the random variations of strand overlaps, the manner in which voids are removed with increase in density is highly nonuniform. Figure 2 shows a schematic of a model mat, which consists of columns of overlapped strands. The number of strand overlaps in each column i and its corresponding column area a_i vary, and are characterized by the Poisson distribution (Eq.1). During the early stage of mat consolidation, only those columns of high strand overlaps are under compression. As the mat thickness T further decreases, those columns will encounter greater compression, whereas the columns of fewer strands may realize lower compression and accordingly some columns may have no compression. It is intuitive that the compression will remove the voids between strands and the greater the compression, the lower the void volume. On the other hand, large voids must exist between strands in the uncompressed columns.

To help model the void formation, we classify the voids between strands into two types: *non-*

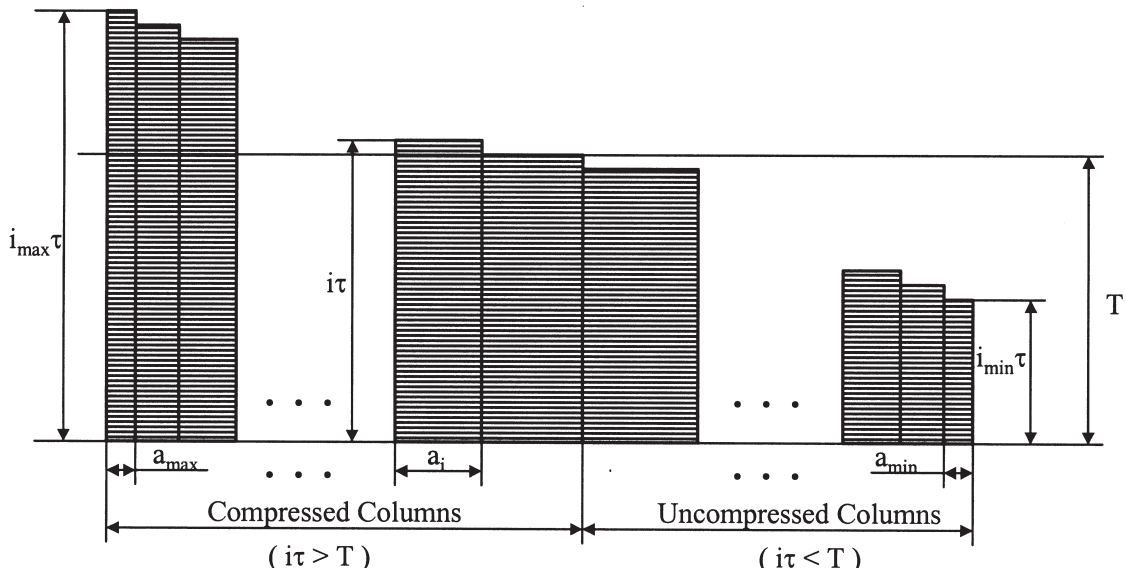

FIG. 2. Schematic of a model mat consisting of columns of overlapping strands characterized by a Poisson distribution (Eq. 1). Note that i = strand overlaps, i_{max}, i_{min} = maximum and minimum strand overlaps, a_i, a_{max} and a_{min} = sum of the mat areas containing respectively i, i_{max} and i_{min} strands, τ = strand thickness, and T = mat thickness.

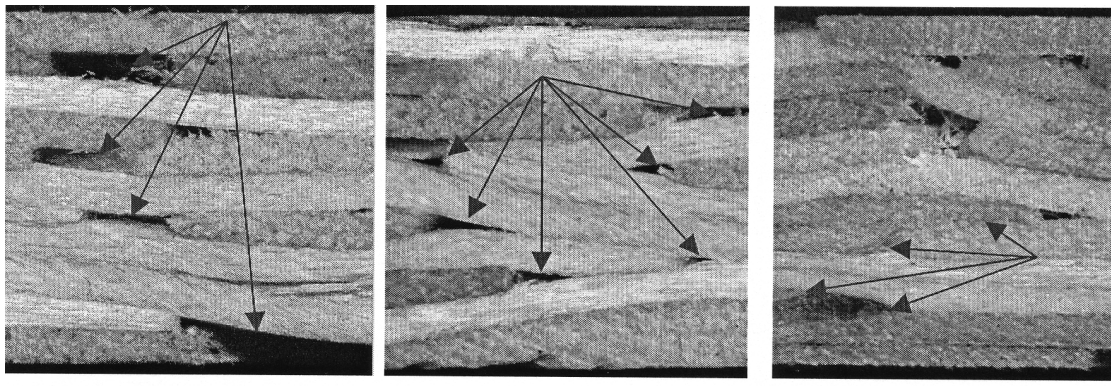

FIG. 3. Photograph pictures of strand mat cross-sections showing the void structure: a) non-contact voids, b) partially filled edge voids, and c) completely filled edge voids.

contact voids and *edge voids*. The non-contact voids exist due to lack of strand-to-strand contacts in the *uncompressed* columns, which symbolize the local mat areas with relatively low numbers of strand overlaps (Fig. 3a). The edge voids are induced by strand edges in the *compressed* columns, which represent the local mat areas with high numbers of strand overlaps (Fig. 3b). In our initial analysis (Dai and Steiner 1993), we assumed that mats contain only the non-contact voids. This may have led to underestimation of the between-strand porosity. Modifications are made herein to include the voids induced by strand edges. This modification will allow for proper consideration of the effects of strand geometry, particularly the strand length and width.

Porosity model for non-contact voids.—For a mat of thickness T, non-contact voids only exist in those columns or mat areas with overlap number i less than T/τ. Therefore, the corresponding void volume equals $(T-i\tau)\, a_i$ and the porosity is $(T-i\tau)\, a_i /(TA)$. For all the columns with overlap number less than T/τ, the porosity for non-contact voids $\phi_{b,n}$ is:

$$\phi_{b,n} = \frac{1}{TA} \sum_{i=0}^{T/\tau} (T - \zeta i\tau) a_i \qquad (8)$$

Substituting a_i/A in Eq. (8) with Eq. (1) yields:

$$\phi_{b,n} = \frac{e^{-n}}{T} \sum_{i=0}^{T/\tau} (T - \zeta i\tau) \frac{n^i}{i!} \qquad (9)$$

where ζ = roughness coefficient. This is to take into account the existence of micro-voids between contacts of nominally flat strand surfaces (Knudson et al 1999). Depending upon the surface roughness, ζ varies from 0.8 to1.0 with unity representing perfectly smooth strands.

Porosity model for edge voids.—In the compressed columns, triangular voids often exist around the strand edges (Fig. 3b). The size of the triangular voids is likely controlled by the strand thickness τ and lateral expansion of strands due to compression. As they are compressed in thickness direction, the strands will expand in length and width directions. While it can be largely contained by strand-to-strand surface contact, the lateral expansion encounters much less constraint around the edges. Depending upon the compression, the edge expansion coupled with bending deformation of the adjacent strands may partially fill or completely eliminate the edge voids (Fig. 3c). In a partially filled case, the void volume can be calculated by subtracting the area of the parabolic expansion, $S_{e,i}$ [m^2], from that of the triangle ΔABC, $S_{t,i}$ [m^2], assuming their depths are the same (Fig. 4).

Let us first calculate the triangle area $S_{t,i}$. As shown in Figs. 3b and 4, the baseline length of

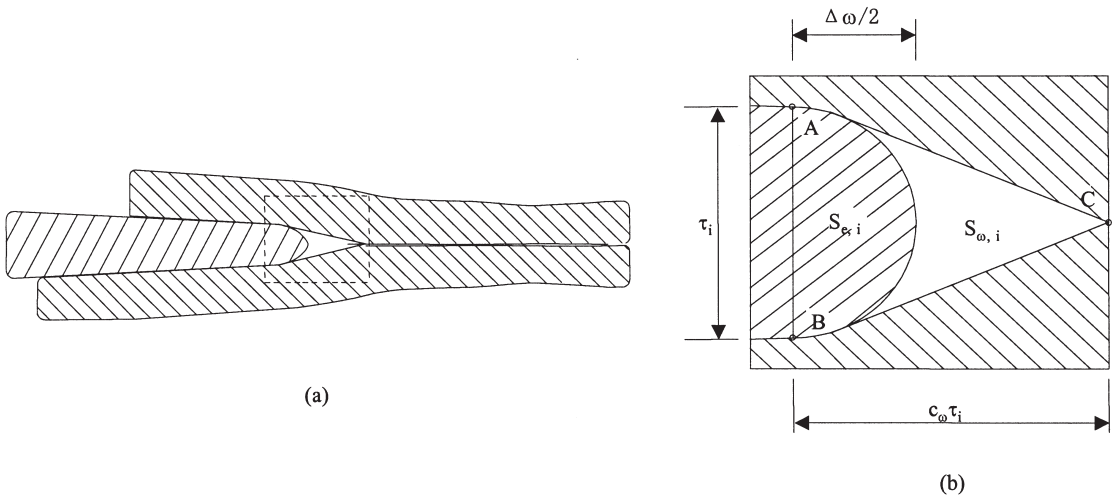

FIG. 4. Schematic of a cross-section of strand overlaps and an edge void: a). overlaps between three strands with squared area of interest, and b). enlarged cross-section showing the dimensions of an edge void.

the triangles equals compressed strand thickness τ_i. Here the subscript i denotes the compressed strand thickness in columns of i overlapping strands. While it likely depends on the deflection of crossing strands and mat densification, the height of the triangle is assumed to be proportional to the baseline length (strand thickness). The triangle area, $S_{t,i}$, is then given by:

$$S_{t,i} = \frac{c_\omega}{2}\tau_i^2 \tag{10}$$

where: c_ω = an adjusted coefficient, which is further given by: $c_\omega = (\omega/\omega_r)^{0.5}$. Here ω_r is a reference strand width for normalization (e.g., 0.025 m). This adjustment is made based on our early study, which showed that the distances between strand crossings were correlated to the strand width in the width direction (Dai and Steiner 1994a). In Eq. (10), the compressed strand thickness is given by: $\tau_i = T/i$.

For a strand column with strand overlaps i, its compression strain ε_i is given by:

$$\varepsilon_i = \frac{\tau - \tau_i}{\tau} = 1 - \frac{T}{i\tau} \tag{11}$$

The expansion in the strand width direction $\Delta\omega$ [m] is:

$$\Delta\omega = \mu_\omega \varepsilon_i \omega \tag{12}$$

where μ_ω = Poisson ratio for the strand width direction (approximately 0.05, which is low due to surface constraints).

The expansion area $S_{e,i}$ is:

$$S_{e,i} = \frac{2}{3}\tau_i \frac{\Delta\omega}{2} = \frac{1}{3}\tau_i \mu_\omega \varepsilon_i \omega \tag{13}$$

where $\Delta\omega$ is given by Eq. (12).

Combining Eqs. (10), (11), and (13), we get the void area along the strand width $S_{\omega,i}$ [m^2]:

$$S_{\omega,i} = S_{t,i} - S_{e,i} = \frac{c_\omega}{2}\left(\frac{T}{i}\right)^2 - \frac{1}{3}\left(\frac{T}{i}\right)\mu_\omega\left(1 - \frac{T}{i\tau}\right)\omega \tag{14}$$

Note that a void exists only if $S_{\omega,i} > 0$ (Fig. 3b). If $S_{\omega,i} \leqslant 0$, a void is nonexistent (Fig. 3c).

Similarly, the void area along the strand length $S_{\lambda,i}$ [m^2] is:

$$S_{\lambda,i} = \frac{c_\lambda}{2}\left(\frac{T}{i}\right)^2 - \frac{1}{3}\left(\frac{T}{i}\right)\mu_\lambda\left(1 - \frac{T}{i\tau}\right)\lambda \approx \frac{c_\lambda}{2}\left(\frac{T}{i}\right)^2 \tag{15}$$

where zero lateral expansion is assumed in the length (grain) direction, or $\mu_\lambda = 0$. Similar to Eq. (10), the adjusted coefficient in the length direction is given by: $c_\lambda = (\lambda/\lambda_r)^{0.5}$. Parameter λ_r is a reference strand length for normalization (e.g., 0.1 m).

For a single strand, its edge voids exist along the sides of length and width. While the cross-section areas of the voids are given by Eqs. (14) and (15), the depth of the voids should be determined by the strand length and width. Accordingly, the volume of the voids is $2(S_{\omega,i}\lambda + S_{\lambda,i}\omega)$ [m^3].

For all strands in the i overlap columns, the total volume of the edge voids is $2(S_{\omega,i}\lambda + S_{\lambda,i}\omega) N_f p(i)$. Since the edge voids only exist in columns under compression or in which strand overlap i is: $\geq T/\tau + 1$, the porosity $\phi_{b,e}$ is then given by:

$$\phi_{b,e} = \frac{2N_f}{TA} \sum_{i=T/\tau+1}^{\infty} \left(S_{\omega,i}\lambda + S_{\lambda,i}\omega\right) p(i) \quad (16)$$

where: $p(i)$ is the Poisson variable defined by Eq. (1).

Combining with Eqs. (1) and (2), Eq. (16) can be rewritten as:

$$\phi_{b,e} = \frac{2e^{-n}n}{T} \sum_{i=T/\tau+1}^{\infty} \left(\frac{S_{\omega,i}}{\omega} + \frac{S_{\lambda,i}}{\lambda}\right) \frac{n^i}{i!} \quad (17)$$

Finally, the total porosity between strands ϕ_b including both the non-contact voids $\phi_{b,n}$ (Eq.9) and edge voids $\phi_{b,e}$ (Eq.17) can be readily obtained by:

$$\phi_b = \phi_{b,n} + \phi_{b,e} \quad (18)$$

Mat permeability

Classic model for porous media.—Permeability is a very important property of porous media, which cover a wide range of materials including soil, rock, and beds of natural or synthetic particles and fibers. Therefore, the subject of permeability has been widely investigated and an enormous amount of knowledge has been accumulated (Dullien 1992). Among all the models that have been developed, the Carman-Kozeny model (Carman 1956 and Kozeny 1927) is probably the most popular. Based on the analogy of flow through hydraulic channels, the generic form of the Carman-Kozeny equation for permeability k_{CK} [m^2] is:

$$k_{CK} = \frac{\phi^3}{k'\left(1-\phi\right)^2 S_0^2} \quad (19)$$

where: ϕ = porosity,
S_0 = specific surface area based on solid's volume [m^{-1}], and
$k' = k_0(L_e/L)^2$, which is often referred to as Kozeny constant or tortuosity. Further k_0 is a constant, and L_e and L are the effective microscopic flow length and the macroscopic flow length, respectively.

Note that the permeability as analyzed here is a property of macroscopic flow. According to Carman (1956), the macroscopic flow is obtained by fluid particles actually traveling along a microscopic path length L_e which is always longer than the shortest distance along the macroscopic direction L. The Kozeny constant k' is a measure of how long the effective microscopic flow path length L_e is compared to the macroscopic flow path length L. Unfortunately, the value L_e or L_e/L is seldom known. The best value for k' to fit most experimental data on packed beds of spheres is equal to 5. Assume particles can be approximated in shape by spheres. The specific surface area is then given by:

$$S_0 = \frac{\pi D_p^2}{\pi D_p^3/6} = \frac{6}{D_p} \quad (20)$$

and the common form of Carman-Kozeny for beds of particles then becomes:

$$k_{CK} = \frac{D_p^2\phi^3}{180\left(1-\phi\right)^2} \quad (21)$$

where: D_p = equivalent sphere diameter [m].

The Carman-Kozeny equation (Eq.21) has been found particularly useful for most packed particles or fibers (Dullien 1992). However, it

may not be valid for particles that deviate significantly from the spherical shape or consolidated media. Indeed, a consolidated mat of wood strands deals with neither spherical particles nor a loosely packed structure. Therefore, modifications must be made before the Carman-Kozeny model can be applied.

Model for strand mats.—To apply the Carman-Kozeny theory to wood composites, it is first hypothesized that the flow occurs only in voids between strands and the flow through wood is negligible. Under this assumption, only the between-strand porosity ϕ_b (Eq. 18) should be considered.

Secondly, the Carman-Kozeny model is modified to account for the strand shape and the mat consolidation. Assume strands are rectangular in shape. Their specific surface area based on the solid's volume S_1 [m^{-1}] is:

$$S_1 = \frac{2(\lambda\omega + \lambda\tau + \omega\tau)}{\lambda\omega\tau} = 2\left(\frac{1}{\tau} + \frac{1}{\omega} + \frac{1}{\lambda}\right) \qquad (22)$$

For OSB strands, the length λ and the width ω are usually an order of magnitude greater than the thickness τ. Equation (22) can therefore be approximated by:

$$S_1 \approx \frac{2}{\tau} \qquad (23)$$

When a mat is consolidated, the strand thickness decreases. Due to the random variation, the thickness changes also vary. The effective strand thickness τ_e [m] at a given mat thickness or density is given by:

$$\tau_e = \sum_{i=0}^{T/\tau} \tau p(i) + \sum_{i=T/\tau+1}^{\infty} \frac{T}{i} p(i) \qquad (24)$$

Combining with Eq. (1), Eq. (24) becomes:

$$\tau_e = e^{-n}\left(\sum_{i=0}^{T/\tau} \tau \frac{n^i}{i!} + \sum_{i=T/\tau+1}^{\infty} \frac{T}{i}\frac{n^i}{i!}\right) \qquad (25)$$

Similar to Eq. (23), the effective specific strand surface area available for flow S_e [m^{-1}] is:

$$S_e = \frac{2}{\tau_e} \qquad (26)$$

Finally, by combining Eq. (26) with Eq. (19), the modified Carman-Kozeny equation for predicting permeability of wood composite mats k [m^2] becomes:

$$k = \frac{\tau_e^2 \phi_b^3}{c'\left(1-\phi_b\right)^2} \qquad (27)$$

where: c' = tortuosity constant, which is determined for best fit with experimental data. Since strand mats are layered in structure, the transverse permeability k_T is different from the lateral permeability k_L. The difference between k_T and k_L will lie in their corresponding values of the constants c'_T and c'_L.

Thus, a fundamental model for mat permeability has been developed based on the classic Carman-Kozeny theory and the mat structure. This model has for the first time linked the mat permeability to such important parameters as mat porosity (mat densification) and strand dimensions.

EXPERIMENTAL TESTS

There were two basic objectives for conducting the experimental tests: to validate the hypothesis that mat permeability is affected mainly by between-strand porosity and to validate the permeability model. The first objective was achieved by comparing the permeability of mats with that of solid wood of which the mats were composed. To meet the second objective, permeability of mats of various strand dimensions were tested and compared with the model predictions.

Materials

To insure accurate results on the effects of strand dimensions, uniform strands were prepared. Aspen (*Populus tremuloides*) logs were first peeled using a rotary lathe into smooth veneer of intended thickness. The veneer was further dried and cut into rectangular strands of uniform length and width. Five strand dimensions were chosen as shown in Table 1. The di-

TABLE *1. Strand dimensions used for the permeability tests.*

Test No.	Length (mm)	Width (mm)	Thickness (mm)
1	50.8	25.4	0.75
2	101.6	25.4	0.75
3	152.4	25.4	0.75
4	50.8	6.3	0.75
5	50.8	6.3	1.05

mensional combinations enabled the effects of all three strand-dimensions (thickness, width, and length) to be examined within the scope of tests. Strands were dried to 5% moisture content on an oven-dry basis, blended with 2% (w/w) powdered phenol-formaldehyde resin and hand-formed to randomly oriented strand mats of 320 mm by 320 mm. The mats were pressed to 10-mm thickness at three target densities: 500, 600, and 700kg/m^3.

Special pressing methods were used to produce homogeneous panel density to minimize the effect of vertical density profile. The mats were pressed at low temperature 75°C until the same temperature was is reached at the core. Then the platen temperature was further increased to 160°C and held at that temperature until the core reached 125°C. The pressing time was around 15 min. A total of nine boards were made with three replicates for each target density. Nine disc specimens of 60 mm in diameter were cut from each board, which yielded a total of 81 samples for the permeability tests.

To compare the permeability of strandboard with solid wood, aspen lumber boards with average density of 410 kg/m^3 were pressed to 10 mm and two target densities: 600 and 700kg/ m^3. After densification, a total of 42 disc specimens of 60 mm in diameter were then cut and subjected to the same permeability tests. Note that only the permeability along the panel thickness (radial) direction was measured.

Procedures

A special device was developed to allow air to flow through the disc specimens and the pressure drop and air flow rate to be measured. According to the principle of the apparatus shown in Fig.5, the permeability was calculated as following:

$$k = \frac{\mu \cdot L \cdot Q \cdot P_2}{F \cdot \Delta P \cdot \overline{P}} \tag{28}$$

where: k = permeability [m^2];
μ = viscosity of fluid [Pa.s], (for air at room temperature $\mu = 1.846 \times 10^{-5}$ Pa • S);
L = length in flow direction ,thickness of specimen [m];
F = cross-sectional area of the specimen [m^2];
Q = volumetric flow rate at pressure P_2 [m^3/s];
ΔP = pressure differential = $P_1 - P_2$ [Pa];
$\overline{P} = (P_1 + P_2)/2$ arithmetic average pressure [Pa];
P_1 = given air pressure [Pa]
$P2$ = pressure at which Q was measured [Pa].

RESULTS AND DISCUSSION

Predicted porosity variations during mat consolidation

Porosity in wood composites is in general highly correlated to product density. While density is easy to measure, porosity is very difficult to quantify especially considering the fact that voids exist both within cellular wood structure and between wood elements. Modeling offers

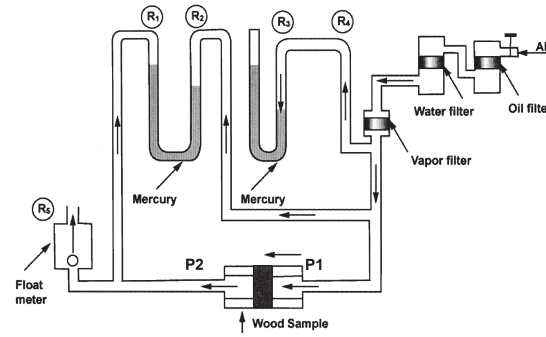

FIG. 5. Schematic of the permeability testing apparatus.

one way to shed insight into the void structure not only in the final product but also during the manufacturing process.

Porosity and density relationship.—Figure 6 depicts the predicted porosity variations in a mat during consolidation. While the total porosity ϕ_t linearly decreases with mat density, the porosity variations inside strands ϕ_i and between strands ϕ_b are noticeably different both in terms of the trend and the magnitude. After forming, a mat of strands is usually very porous due to the existence of voids between strands. These voids, however, can be rapidly eliminated during the early stage of consolidation, as evidenced by a sharp decrease of the between-strand porosity with increase in mat density in Fig. 6. During this stage, the inside-strand porosity increases mainly because the relative volumetric change of the mat with mat density is much greater than that of voids inside strands. In fact, the inside-strand void volume cannot realize a significant decrease until most of the voids between strands are eliminated. The breaking point seems to occur around or shortly after a mat density of 400 kg/m^3 or the original wood density.

Further consolidation leads to a very slow decrease in porosity between strands and a relatively rapid decrease in porosity inside strands. While reduction of voids between strands is necessary to create strand-to-strand contact for bonding (Dai and Steiner 1993), decrease of voids inside strands inevitably leads to densification of wood substance, which ideally should be avoided to maximize volumetric recovery of wood. As shown in Fig. 6, the decrease in porosity after 400 kg/m^3 mat density comes directly at the expense of wood volumetric loss. Currently, most of the strand-type wood composites including particleboard and oriented strandboard require that mat density be around 600 to 800 kg/m^3. At such high densities, not only are the final products significantly heavier than solid wood, but also 40 to 50% of wood volume is lost (Fig. 6). This volumetric loss is substantially high compared to less than 10% loss for veneer-based products. The high loss stems from the discontinuity of strands and the random mat formation. This result suggests the importance of strand preparation and mat formation to producing lower density products.

Non-contact voids vs edge voids.—The voids exist between strands in a mat due to the lack of strand contacts and/or the existence of strand edges. Figure 7 reveals that the non-contact voids dominate during the early stage of mat consolidation. As the mat is further consolidated, localized contacts between strands are developed, resulting in the elimination of large voids. As the voids between strand faces are eliminated, small voids around strand edges start to emerge and eventually dominate in the final porous network. The elimination of the edge voids appears to be difficult (Fig. 7) and inevitably leads to the loss in wood recovery (Fig.6). On the other hand, a small amount of the

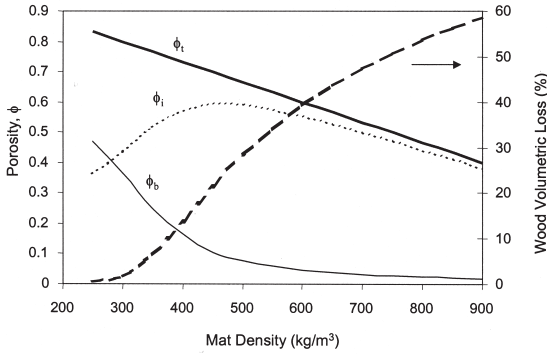

FIG. 6. Typical variations of total porosity ϕ_t, inside-strand porosity ϕ_i, between-strand porosity ϕ_b and volumetric loss of wood during mat consolidation.

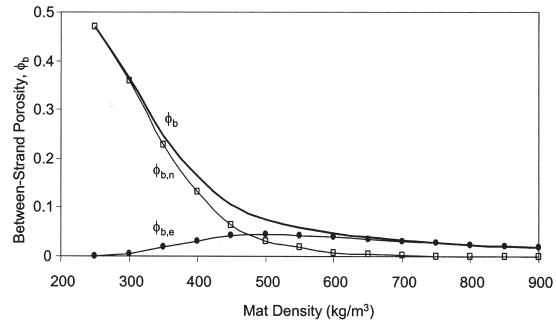

FIG. 7. Typical variations of between-strand porosity ϕ_b, non-contact porosity $\phi_{b,n}$ and edge porosity $\phi_{b,e}$ during mat consolidation.

voids may not be detrimental at all since they can offer passages for gas to flow through the mats during pressing and air/vapor to permeate through the boards in service – an attribute becoming increasingly important to the durability of the building envelop (e.g., Bumbaru et al. 1988).

Effects of strand dimensions on between-strand porosity.—Figures 8 a, b, and c show, respectively, the effects of strand length, width, and thickness on the porosity between strands. For both strand length and width, the porosity decreases as the strand dimensions increase mainly because of the edge effects. The relationships are nonlinear with porosity being more sensitive to changes in length and width when the dimensions are small. The porosity changes little when strands become really long or wide.

In contrast, the relationship between porosity and strand thickness is almost linear and highly positive. The void volume always increases with an increase in strand thickness. According to the model, both non-contact voids and edge voids are highly dependent upon strand thickness (Eqs. 9–17). For this reason, strand thickness has the strongest impact on porosity among all strand dimensions. Strand width also has greater effect than length. These results suggest that one way to manufacture low-porosity products is to use thin and large strands.

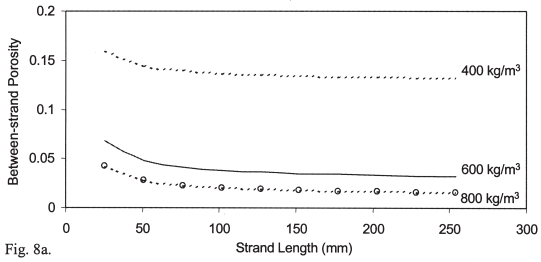

Fig. 8a.

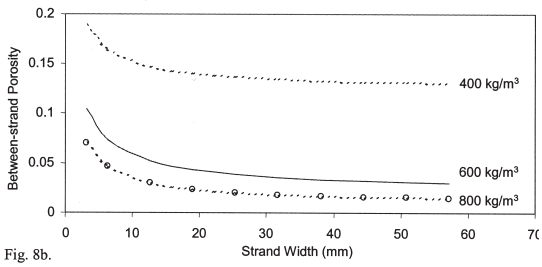

Fig. 8b.

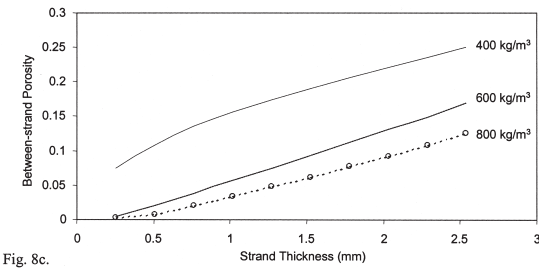

Fig. 8c.

FIG. 8. Effects of strand dimensions on the between-strand porosity: a). Effect of strand length (width: 25.4 mm and thickness: 0.76 mm), b). Effect of strand width (length: 101.6 mm and thickness: 0.76 mm), and c). Effect of strand thickness (length: 101.6 mm and width: 25.4 mm).

Permeability model validations and predictions

Comparing permeability between wood and mat.—A key assumption for this model is that the mat permeability is due to the voids between strands instead of those inside strands. Figure 9 compares the vertical permeability through mat thickness and the transverse (perpendicular-to-grain) permeability of wood. Over the typical density range of mat consolidation, both the mat permeability and the wood permeability decrease in a logarithmically linear manner as seen by the regression lines in Fig.9. The wood permeability is consistently lower by an order of magnitude. This result implies that the flow through wood may indeed contribute very little

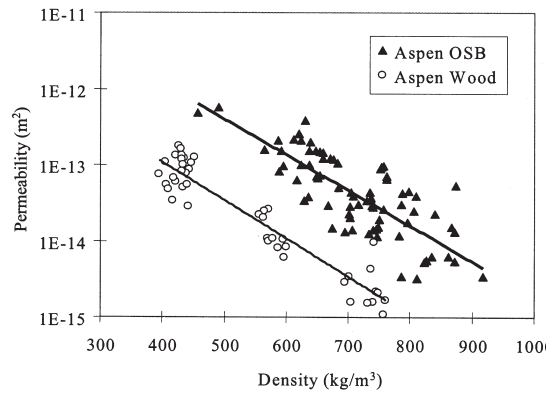

FIG. 9. Logarithmic plot comparing the vertical permeability of aspen OSB boards with the perpendicular-to-grain permeability of aspen wood at various densifications.

to the overall permeability of a mat. It therefore confirms that the flow inside a mat mainly occurs through the voids between strands as opposed to those inside strands.

Model validation.—Because of our equipment limitations, it was difficult to perform the permeability tests without incurring significant errors on mats with density below 450 kg/m^3. As a first validation, we used the data from von Haas (1998), who tested density as low as 300 kg/m^3. Figure 10 compares the model predictions with the experimental data with a remarkably close agreement. Here the tortuosity constant used to fit the experimental data c'_T is 500 (Eq. 27).

To further validate the model, Fig. 11 compares the permeability of mats made of different strand dimensions. The experimental data show considerable variations, which seems consistent with what was reported in the literature (e.g., Bolton and Humphrey 1994). In addition to the natural causes of wood, the permeability variations are likely due to the variations in mat/panel structure and the edge effects of relatively small testing specimens. The mat structural variations can cause variations of both porosity ϕ_b and tortuosity c' (Eq. 27). As far as the edge effect, larger specimen size may yield more consistent results, especially for strandboards. Despite the variations, the trends between the permeability and the strand dimensions seem well predicted by the model.

Relationships between mat permeability and strand dimensions.—Figures 12a, b, and c depict three predicted family curves of mat permeability with respect to strand length, strand width, and strand thickness, respectively. For strand length and width, the larger the dimensions, the lower the permeability. However, the degree with which permeability changes decreases as the dimensions increase. In other words, permeability is more sensitive to small strands than large strands. This result stems from the influence of strand dimensions on between-strand porosity through their edge effects (Fig. 8a and b). Furthermore, strand length and width have diminished effects on permeability at lower density range. During the early stage of consolidation, the mat is highly porous and its porosity structure is governed by the large gaps between strand surfaces instead of the small voids around strand edges. As a result, the mat permeability is very high and should be mainly controlled by mat density.

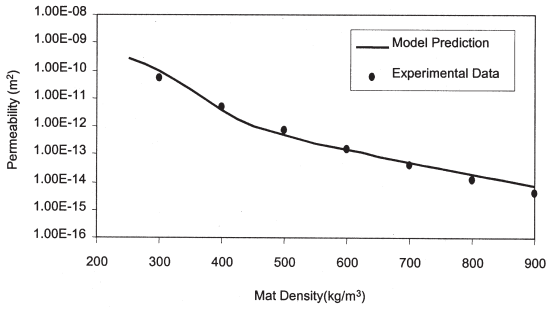

FIG. 10. Logarithmic plots comparing mat vertical permeability between the model prediction and experimental data (Strand length: 30.60 mm, width: 5.10 mm and thickness: 0.62 mm, and c_T'=500).

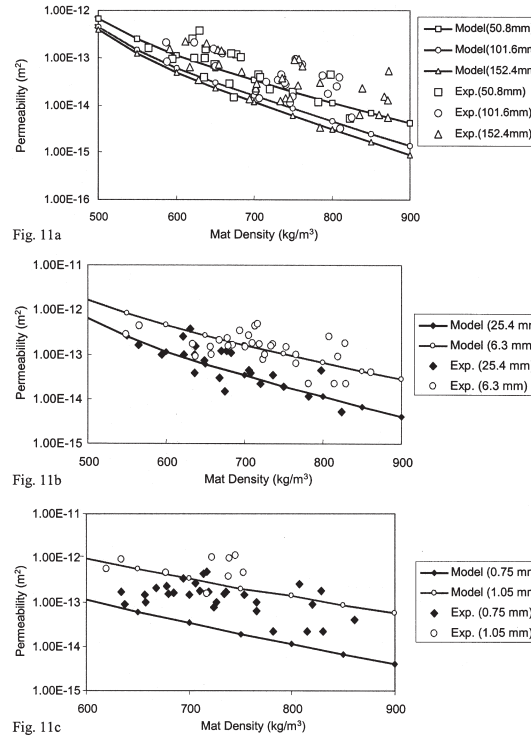

FIG. 11. Logarithmic plots comparing mat vertical permeability between the model prediction and experimental data: a). Effect of strand length, b). Effect of strand width, and c). Effect of strand thickness (See Table 1 for other strand dimensions, and c_T'=500)

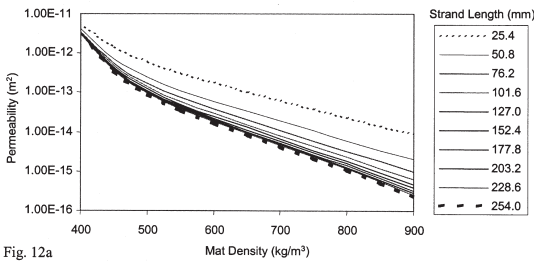

Fig. 12a

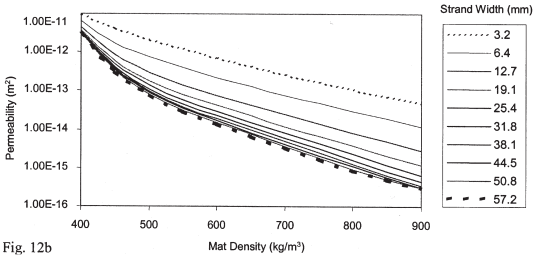

Fig. 12b

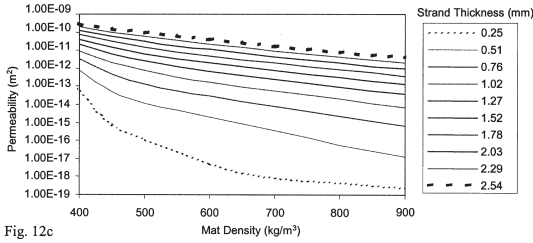

Fig. 12c

FIG. 12. Logarithmic plots showing the relationships between mat vertical permeability and strand dimensions (c_T'=500): a). Effect of strand length (Width: 25.4 mm and thickness: 0.76 mm), b). Effect of strand width (Length: 101.6 mm and thickness: 0.76 mm), and c) Effect of strand thickness (Length: 101.6 mm and width: 25.4 mm).

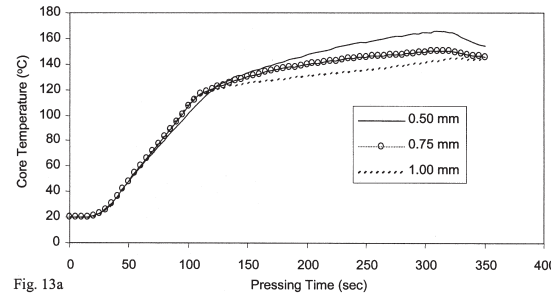

Fig. 13a

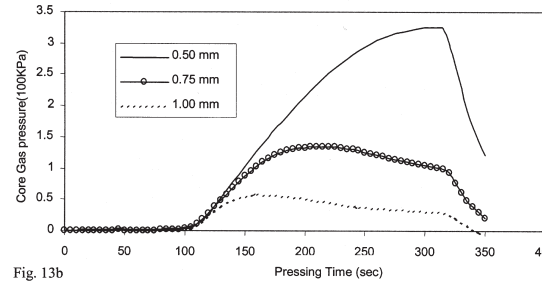

Fig. 13b

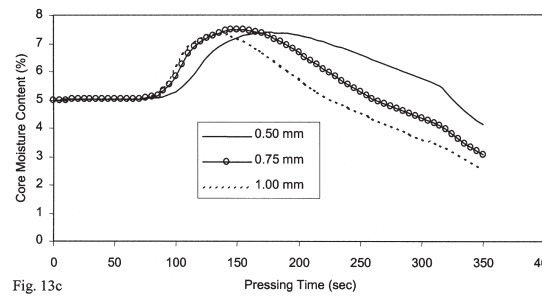

Fig. 13c

FIG. 13. An example of predicted effect of strand dimensions (strand thickness with length fixed at 100 mm and width 25 mm) on heat and mass transfer in strand mats during hot pressing: a). Effect on core temperature, b). Effect on core gas pressure and c). Effect on core moisture content.

Besides mat density, strand thickness is another dominant factor in determining mat permeability. As shown in Fig. 12c, increasing strand thickness significantly increases mat permeability, even at lower mat density. The strong thickness effect is due to its effects on both the between-strand porosity (Fig. 8c) and the strand specific surface area (Eq. 26). It is also interesting to note that similar to strand length and width, strand thickness has a greater effect on mat permeability as strands get thinner.

Effects of strand dimensions on hot pressing

Figure 13 shows an example of how strand dimensions can affect hot-pressing by depicting the variations of core temperature, gas pressure, and moisture content in mats of strands with different thickness during pressing. The results are based on predictions using the heat and mass transfer model developed in the preceding paper (Dai and Yu 2004) and the permeability model described in this paper. It is apparent that strand thickness has a significant impact on all three pressing parameters, particularly the maximum core temperature, the maximum gas pressure, and the final core moisture content. The higher maximum core temperature, higher gas pressure, and higher final core moisture content are all attributed to the thinner strands and hence the

lower permeability (both transverse permeability and lateral permeability).

Likewise, the effects of strand length and width can also be predicted. Due to their effects on permeability, longer or wider strands will lead to higher maximum core temperature, higher core gas pressure, and higher core moisture content. It is worth noting that high core gas pressure often causes problems of "blows" or delaminations. To minimize the "blows," one may need to use lower moisture strands and/or prolong the decompression time when making boards with strands of large dimensions.

SUMMARY AND CONCLUSIONS

Theoretical models are developed for the first time to mathematically characterize the porosity and permeability of wood strand-based composite mats. To facilitate the model development, a strand mat is conceptually visualized as a system of overlapping strand columns. Assuming random mat formation, the strand overlaps in the columns follow a Poisson distribution with its average determined by the product of compaction ratio (mat density over strand density) and thickness ratio (mat thickness over strand thickness). Since wood is a porous material, the void volume inside a mat is composed of voids inside strands and voids between strands. While the total mat porosity is readily given by known density of cell wall, the porosity between strands in a consolidated mat needs to be calculated by taking into account the random variations of strand overlaps and the effects of strand edges. The between-strand void volume is classified into, and calculated by, non-contact voids and edge voids. Besides the Poisson strand overlap variation, other factors such as strand surface roughness and lateral strand expansion are also considered.

According to the model predictions, the total mat porosity linearly decreases with mat density, whereas the between- and inside-strand porosities change in highly nonlinear but distinctly different manners. The results shed important insights into the development of strand-to-strand contact and the loss of wood volume during the course of mat consolidation. The model also predicts the different manners in which mat porosities are affected by strand length, width, and thickness, with the thickness being most significant followed by the width and the length.

With the prior knowledge of mat porosities, the Carman-Kozeny theory for porous material is applied to model the permeability of wood strand composites. Under the assumption that gas flow inside a mat occurs only between strands, the model takes into account the between-strand porosity and the strand specific surface area. Experimental tests are conducted to validate the permeability model. The results reveal that permeability of solid wood is an order of magnitude lower than that of strand mats at the same density. Reasonably good agreements are found between the model predictions and the experimental results. The model predicts different relationships between the mat permeability, the mat density, and the strand dimensions.

Through the model, the variations of core temperature and gas pressure inside a mat during hot-pressing can be successfully linked to the effects of mat permeability, porosity and strand dimensions. This study may provide a theoretical basis for systematic analyses of the processing and properties of wood composites, particularly strand-based products.

ACKNOWLEDGMENT

The authors would like to thank Forintek's industry members, Natural Resources Canada (Canadian Forest Service), and the Provinces of British Columbia, Alberta, Saskatchewan, Manitoba, Quebec, Nova Scotia, New Brunswick, and Newfoundland, and Labrador for their guidance and financial support for this research.

REFERENCES

Bolton, A. J., and P. E. Humphrey. 1994. The permeability of wood-based composite materials. Part 1. A review of the literature and some unpublished work. Holzforschung 48(Suppl.): 95–100.

Bumbaru, D., R. Jutras, and A. Patenaude. 1988. Air permeance of building materials. Canada Mortgage and Housing Corp. Technical Report. 12 pp.

CARMAN, P. C. 1956. Flow of gas through porous media. Butterworths, London, UK.

CARVALHO, L. M. H., M. R. N. COSTA, AND C. A. V. COSTA. 2003. A global model for the hot-pressing of MDF. Wood Sci. Technol. 37(3–4): 241–258.

DAI, C., AND P. R. STEINER. 1993. Compression behaviour of randomly-formed wood flake mats. Wood Fiber Sci. 25(4): 349–358.

———, AND ———. 1994a. Spatial structure of wood composites in relation to processing and performance characteristics. Part II. Modelling and simulation of a randomly-formed flake layer network. Wood Sci. Technol. 28(2): 135–146.

———, AND ———. 1994b. Spatial structure of wood composites in relation to processing and performance characteristics. Part III. Modelling and simulation of a random multi-layered flake mat. Wood Sci. Technol. 28(3): 229–239.

———, AND ———. 1997. On horizontal density variations in randomly-formed short-fibre wood composite boards. Composites Part A. 28(A): 57–64.

———, AND C. Yu. 2004. Heat and mass transfer in wood composite panels during hot pressing: Part 1. A physical-mathematical model. Wood Fiber Sci. 36(4): 585–597.

———, S. CHEN, AND A. PIELASCH. 1996. Simulation of mat formation for strand composites processing. Pages 32–39 *in* Proc. 3rd Pacific Rim Bio-based Composites Symposium. Nov 2–5, 1996. Kyoto, Japan.

DULLIEN, F. A. 1992. Porous media: Fluid transport and pore structure. 2nd ed. Academic Press, New York, NY.

HATA, T., S. KAWAI, R. EBIHARA, AND H. SASAKI. 1993. Production of particleboard with steam injection. Part V. Effect of particle geometry on temperature behavior in particle mats and air permeabilities of boards. Mokuzai Gakkaishi 39(2):161–168.

HUMPHREY, P. E., AND A .J. BOLTON. 1989. The hot pressing of dry-formed wood-based composites. Part II A simulation model for heat and moisture transfer, and typical results. Holzforschung 43(3): 199–206.

KNUDSON, R. M., L. CHEN, P. ENS, AND G. SMITH. 1999. Effect of frozen wood on stranding quality of aspen for OSB. Alberta Research Council. Technical Report. 20 pp.

KOZENY, J. 1927. Uber Kapillare Leitung des Wassers im Boden. Sitzungsberichte der Akadamie der Wissenschaften in Wien, Abteilung, Illa, 136:271–206.

SUCHSLAND, O. 1959. An analysis of the particle board process. Michigan Quart. Bull. 42(2): 350–372.

VON HAAS, G. 1998. Investigations of the hot pressing of wood-composite-mats under special consideration of the compression-behaviour, the permeability, the temperature-conductivity and the sorption-speed (In German). Ph.D thesis, University of Hamburg, Germany.

WU, Q., AND J. N. LEE. 2002. Predicting the influence of voids on the engineering constants of oriented strandboard: a continuum model. Pages 372–380 *in* Proc. 6th Pacific Rim Bio-based Composites Symposium. Portland, OR.

ZOMBORI, G .B., F. A. KAMKE AND L. T. WATSON. 2003. Simulation of the internal conditions during the hot-pressing process. Wood Fiber Sci. 35(1): 2–23.

APPENDIX: ERRATA FOR PART 1

Editorial errors were noticed with Equations 4 and 8f in part 1 of this publication series (Dai and Yu 2004). The correct equations should be:

Equation 4:

$$\frac{\partial \varepsilon \rho_v}{\partial \tau} + \frac{\partial \rho_v u_{xg}}{\partial x} + \frac{\partial \rho_v u_{yg}}{\partial y} + \frac{\partial \rho_v u_{zg}}{\partial z} = \dot{E}_{evap}$$

or

$$\frac{\partial \varepsilon \rho_v}{\partial \tau} = \dot{E}_{evap} - \frac{\partial \rho_v u_{xg}}{\partial x} - \frac{\partial \rho_v u_{yg}}{\partial y} - \frac{\partial \rho_v u_{zg}}{\partial z} \tag{4}$$

Equation 8f:

$$\begin{aligned} k_{mat,x} &= (1-\varepsilon)k_{sx} + \varepsilon k_g \\ k_{mat,y} &= (1-\varepsilon)k_{sy} + \varepsilon k_g \\ k_{mat,z} &= (1-\varepsilon)k_{sz} + \varepsilon k_g \end{aligned} \tag{8f}$$